Supporting Information for "Record-low Arctic stratospheric ozone in 2020: MLS observations of chemical processes and comparisons with previous extreme winters"

Gloria L Manney[1,2], Nathaniel J Livesey[3], Michelle L Santee[3], Lucien Froidevaux[3], Alyn Lambert[3], Zachary D Lawrence[4,1], Luis F Millán[3], Jessica L Neu[3], William G Read[3], Michael J Schwartz[3], Ryan A Fuller[3]

[1]NorthWest Research Associates, Socorro, NM, USA

[2]New Mexico Institute of Mining and technology, Socorro, NM, USA

[3]Jet Propulsion Laboratory, California Institute of Technology, Pasadena, CA, USA

[4]National Oceanic and Atmospheric Administration / Cooperative Institute for Research in Environmental Sciences, Boulder, CO, USA

Contents of this file

Introduction

The supplementary text provides further details of the Aura Microwave Limb Sounder (MLS) "Level 3" datasets and access (Text S1), brief descriptions of the "raw" MLS maps and profiles shown in Figs. S1 through S3 (Text S2), and details of the methods for empirical ozone loss

estimates summarized in the main text (Text S3). The supplementary figures show maps of MLS extreme trace gas values taken directly from MLS Level 2 Geophysical Product (L2GP) data (Figs. S1 and S2) (related to Fig. 1 in the main text), minimum O_3 profiles taken directly from MLS L2GP data (Fig. S3) (related to Fig. 3 in the main text), and illustrations of details of "Match" empirical ozone loss estimates (Figs. S4 and S5) (described in Text S3, and related to Fig. 3 in the main text).

Text S1. MLS Level 3 Dataset and Details

The data used to make the maps shown in Fig. 1 in the main text are MLS "Level 2" (L2) data, which are daily data along the orbit tracks and on retrieval pressure levels. The Aura MLS science team has recently made public a "Level 3" (L3) dataset, described in more detail in Livesey et al. (2020). These products include daily and monthly binned values in several views, including "zonal" means in both geodetic (on retrieval pressure levels and potential temperature surfaces) and equivalent (on potential temperature surfaces) latitude, and the vortex averages used herein. These L3 products are now available as part of the MLS datasets from the NASA Goddard Space Flight Center Earth Science Data and Information Services Center (GES-DISC), at https://disc.gsfc.nasa.gov/datasets?page=1&keywords=AURA%20MLS. For the vortex averages in the L3 products, the vortex edge is defined using the altitude-dependent scaled potential vorticity (sPV) profile shown by Lawrence, Manney, and Wargan (2018), which was determined from a climatological average over the extended cold season of sPV values at the equivalent latitude of the maximum PV gradients. Lawrence and Manney (2018) discuss considerations related to different choices of vortex edge definition and show that this choice is robust over the season, including in the fall and spring when many other methods have difficulties.

The equivalent latitude / time series shown in Fig. 2 in the main text are from an internal L3 product produced by the MLS team that is similar to the publicly available L3 products but that has the bin averages weighted by "distance" in time and equivalent latitude from the bin centers and by the MLS L2 precision information. These products have previously been used and are described in numerous studies (e.g., Manney et al., 2015, and references therein).

Text S2. MLS Extreme Values from Level 2 Maps and Profiles Description

Figures S1 and S2show maps at 68 and 46 hPa of extreme values (maxima for ClO, minima for the other species) in MLS data obtained from the L2 profiles on retrieval pressure levels during January through early April in 2020, 2016, and 2011, giving a view of the raw data represented in the snapshots on isentropic surfaces shown in Fig. 1 in the main text. The maps are on a $4^\circ \times 2^\circ$ longitude-latitude grid and are produced by first applying a 3-point median filter to the daily L2GP MLS along-track trace gas values and then finding the extreme values occurring within each mapped spatial bin over the day 1 to 114 time period. The median filter provides a reduction in the visible spatial speckle (i.e. pixel to pixel noise) in the extreme value maps, but the results are not critical to the application of this process. The 3-point along-track filter extends over a spatial distance of about 500 km and is comparable to the spatial mapping scale. Consistent with the isentropic maps shown in the main text, 2016 has the lowest H_2O values (near 3 ppmv at 46 hPa), lower HNO_3 values than in 2011, and those low values (near zero) over a larger area/time than in 2020. Similar maximum ClO (over 2 ppbv) and minimum HCl (near zero) abundances are seen in each year, but the extremes are more frequent in 2011 and 2020 than in 2016, and they cover a larger region in 2020 than in 2011. Minimum ozone

values are clearly much lower in 2020 than in 2011 (near 0/0.2 ppmv in 2020 and 0.9/0.7 ppmv in 2011 at 68/46 hPa).

Figure S3 further defines these minimum ozone values, showing that the lowest minima observed in 2011 were near 0.5 ppmv, compared with less than 0.1 ppmv in 2020. Of course, the true minimum for 2011 might have occurred during the data gap, but the 2020 minimum values on dates before and after the data gap in 2011 are also on the order of 0.5 ppmv lower than those in 2011. The lower stratospheric ozone decrease in this time period is not very different between 2020 and 2011. Because the 1 February minimum values were lower in 2020 than in 2011 (because of early onset of chemical loss, see main text), the profiles shown here suggest a similar rate of chemical ozone loss in February and March in the two years, consistent with the Match estimates shown below and in the main text.

The minimum ozone values shown here are consistent with results from a comparison of ozonesonde and MLS minimum ozone values for 2020, 2016, and 2011 (Ingo Wohltmann, personal communication).

Text S3. Empirical Ozone Loss Estimates Description

Empirical ozone loss estimates for 2020 and 2011 are done using several previously documented methods. In Fig. 3 we showed summary results of the MLS Match method described by Livesey, Santee, and Manney (2015). A few small changes have been made relative to that work: MERRA-2 rather than earlier GEOS-5.1/GEOS-5.2 data are used to drive the trajectory calculations. The vortex edge is now (here and throughout this paper) defined using the values from the potential temperature dependent profile of sPV (from Lawrence et al., 2018) used elsewhere in the paper; however, for the Match calculations, we add $+0.2\times10^{-4}\mathrm{s}^{-1}$ at each

level to those values to minimize the possible impact of mixing across the vortex edge on the calculations. A limit of 10% on the change in sPV values along each trajectory is used (rather than the 25% mainly used by Livesey et al., 2015). Livesey et al. (2015) describe sensitivity tests for the vortex edge and sPV change parameters – in general, their results show that both of these changes tend to select for parcels that are farther inside the vortex, and thus it is not surprising that they often lead to slightly larger estimates of ozone loss (because they are expected to be less affected by any errors related to mixing across the vortex edge). Figures S4 and S5 illustrate the steps in the Match method that lead to the chemical ozone loss estimates shown in the main text, and show the details of the results for 2019/2020 and 2010/2011. The vortex area indicates the averaging region and the area within which the matches are identified. Since the reactions that destroy ozone depend on sunlight, the ozone hourly rate of change is computed per sunlit hour based on all the matches; the daily rate of change and cumulative change are then integrated from the hourly rate. To help assess the uncertainty in transport, a similar procedure is done for N_2O (shown in Figs. S4 and S5, panels f and g), except the rate does not take into account sunlit time. In both cases shown here, above 450 K, the Match procedure erroneously reports a "loss" in mid-stratosphere N_2O, suggesting (as discussed by Livesey et al., 2015) that it either underestimates descent (which would tend to result in underestimating the amount of chemical ozone loss) or overestimates mixing-in of higher N_2O extra-vortex air (the impact of which on inferred ozone loss is less clear, since the morphology of ozone with respect to the vortex edge varies with altitude and time such that it is not obvious whether mixing into the vortex would always decrease or increase ozone). Livesey et al. (2015) found that MLS Match results tended to be at the low end of ozone loss estimates compared to studies using other

methods and/or datasets. However, later study showed that Match-based ozone loss estimates (such as those in this paper) using MERRA-2 rather than GEOS-5.1/GEOS-5.2 analysis fields are more in line with estimates using other techniques.

Figs. S4g and S5h show very similar amounts of ozone loss in 2020 and 2011 up through late March, but, consistent with the observed ozone profiles, with the peak chemical loss at lower altitude in 2020 than in 2011. A slightly earlier onset of chemical loss in 2020 is indicated, but significant ozone loss is not apparent before January, unlike the estimates based on vortex averaged descent described below. The vortex in the middle and upper stratosphere began to erode in late March (Lawrence et al., 2020, also seen here in N_2O in Fig. 3 in the main text), and Fig. S4 shows that the "inner vortex" for the Match averages becomes undefined at the highest levels shown. While "chemical" ozone change appears to decrease (except at the lowest levels shown) in April 2020, N_2O changes indicate increasing errors in transport that would be consistent with this, suggesting (consistent with chlorine being deactivated by this time) that chemical ozone loss ceased by about the end of March.

"Vortex-average descent methods" use a vortex-averaged ozone profile from observations at the beginning and end of the calculation period and an estimate (which can be obtained by several means) of vortex-averaged diabatic descent rates to estimate the ozone amount if the initial observation-based ozone values descended in the vortex via passive transport; the difference between this and the ozone profile at the end of the calculation then gives an estimate of the chemical loss (e.g., Griffin et al., 2019, and references therein). We used two means to estimate the diabatic descent rates here: First, we calculated the temporal and vertical (with respect to potential temperature) gradients of vortex averaged MLS N_2O and used those to estimate the

rate at which it descended. Second, we ran back trajectories (using MERRA-2 fields) for dense grids of parcels from a set of "final" dates and averaged the descent of the parcels that were inside the vortex on those final dates for each earlier day in the run. For these calculations, parcels were initialized on a dense ($0.5^\circ \times 0.5^\circ$) equal-area grid encompassing mid- to high-latitudes, and run back for 90–150 days; the potential temperature of the parcels inside the vortex is then averaged for each day of the runs, giving an estimate of the descent over the period. We used the trajectory code described by Livesey et al. (2015) and Manney and Lawrence (2016, and references therein). The approach using N_2O ends up being limited in the vertical levels and time periods where reasonable estimates can be made because over the course of the winter N_2O descends far enough that near-zero values occupy most of the stratosphere, and only the lowest part of the stratosphere (below 500 K by late March 2020, a slightly higher level in 2011) has N_2O gradients strong enough that they can be used to track descent. Because of the particularly low N_2O values that were descending to the lower stratosphere in 2019/2020 (see Figs. 3 and 4 in main text), these estimates are even more limited during that year than during 2011. On the other hand, the trajectory-based descent grows increasingly more uncertain as the earliest date (the end date of the trajectory runs) is farther back, thus making results for the longer calculations even more uncertain. Furthermore, results from both methods are less certain when the vortex is less strong / well-confined, hence in November and April. Nevertheless, results from these two approaches for vortex averaged descent are generally consistent for the times / levels where both can be and were calculated. These estimates are slightly lower than those from the Match method because they are done using vortex averages over the full, rather than the inner,

vortex region, and so include regions near the edge where the chemical loss signature may be diluted by mixing.

While we get fairly consistent results from each of the empirical ozone loss estimates we have made, particularly for the December through March period when the bulk of the chemical ozone loss takes place, it should be noted that there are large uncertainties in all methods of estimating ozone loss from observations (as discussed in some detail by Livesey et al., 2015; Griffin et al., 2019, and references therein). Comparison with results using other methods and datasets (to appear in this special collection) will be invaluable.

References

Griffin, D., Walker, K. A., Wohltmann, I., Dhomse, S. S., Rex, M., Chipperfield, M. P., ... Tarasick, D. (2019). Stratospheric ozone loss in the Arctic winters between 2005 and 2013 derived with ACE-FTS measurements. *Atmos. Chem. Phys.*, *19*(1), 577–601. Retrieved from https://www.atmos-chem-phys.net/19/577/2019/ doi: 10.5194/acp-19-577-2019

Lawrence, Z. D., & Manney, G. L. (2018). Characterizing stratospheric polar vortex variability with computer vision techniques. *Journal of Geophysical Research: Atmospheres*, *123*(3), 1510–1535. Retrieved from http://dx.doi.org/10.1002/2017JD027556 (2017JD027556) doi: 10.1002/2017JD027556

Lawrence, Z. D., Manney, G. L., & Wargan, K. (2018). Reanalysis intercomparisons of stratospheric polar processing diagnostics. *Atmos. Chem. Phys.*, *18*, 13547–13579. doi: 10.5194/acp-18-13547-2018

Lawrence, Z. D., et al. (2020). *The remarkably strong Arctic stratospheric polar vortex of*

winter 2020: Ties to record-breaking Arctic oscillation and ozone loss. (to be submitted to JGR for this special collection)

Livesey, N. J., Read, W. G., Wagner, P. A., Froidevaux, L., Lambert, A., Manney, G. L., ... Lay, R. R. (2020). *EOS MLS version 4.2x level 2 and 3 data quality and description document* (Tech. Rep.). JPL. (Available from http://mls.jpl.nasa.gov/)

Livesey, N. J., Santee, M. L., & Manney, G. L. (2015). A Match-based approach to the estimation of polar stratospheric ozone loss using Aura Microwave Limb Sounder observations,. *Atmos. Chem. Phys.*, *15*, 9945–9963.

Manney, G. L., & Lawrence, Z. D. (2016). The major stratospheric final warming in 2016: Dispersal of vortex air and termination of Arctic chemical ozone loss. *Atmos. Chem. Phys. Disc.*, *16*. Retrieved from `http://www.atmos-chem-phys-discuss.net/acp-2016-633/` doi: 10.5194/acp-2016-633

Manney, G. L., Lawrence, Z. D., Santee, M. L., Livesey, N. J., Lambert, A., & Pitts, M. C. (2015). Polar processing in a split vortex: Arctic ozone loss in early winter 2012/2013. *Atmos. Chem. Phys.*, *15*, 4973–5029.

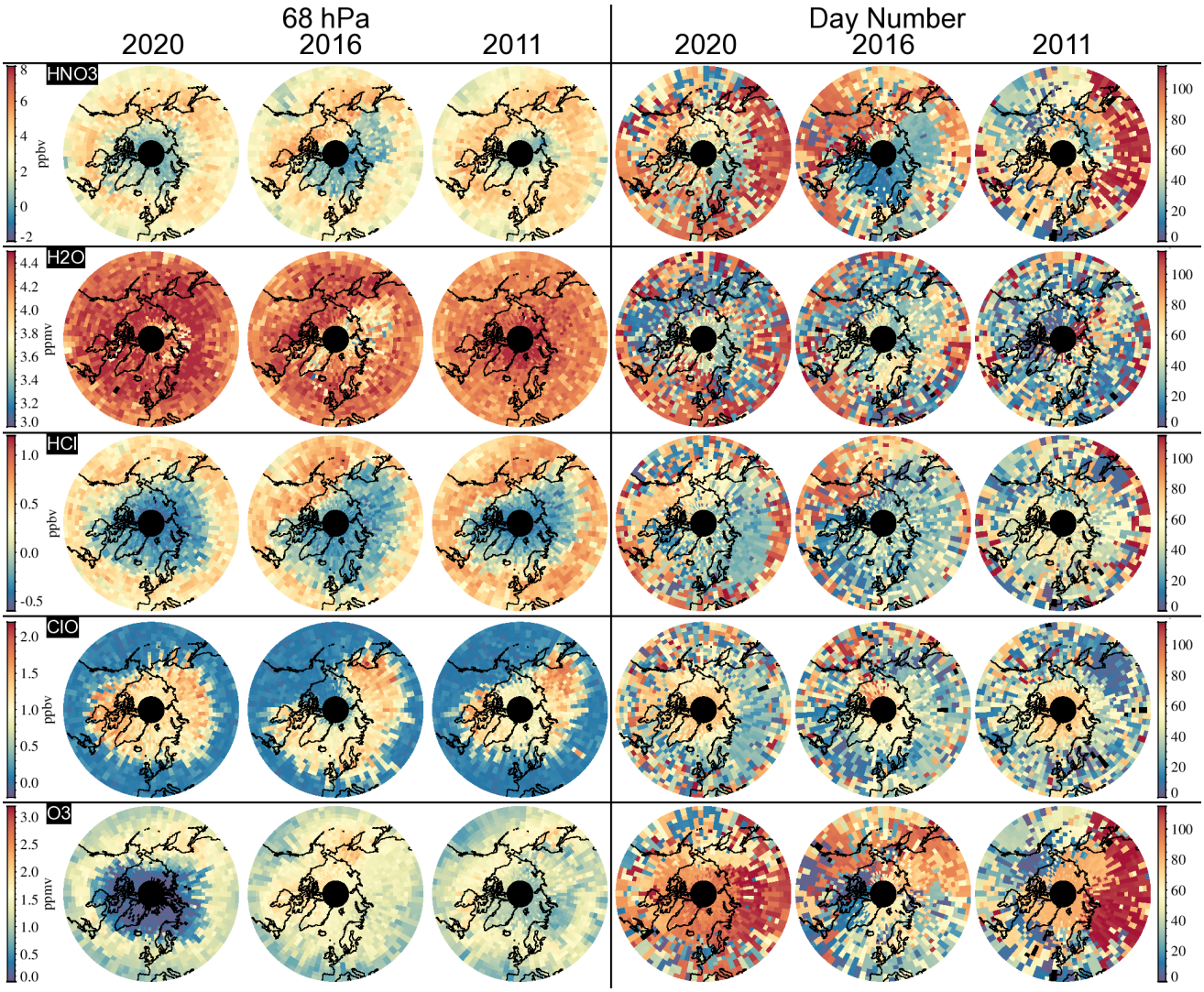

Figure S1. (Left columns) Maps of extreme MLS trace gas values for selected species at 68 hPa during January through early April in 2020, 2016, and 2011. Extrema are maxima for ClO and minima for all the other species shown. (Right columns) Corresponding maps of the day of occurrence (day number) of the extreme values.

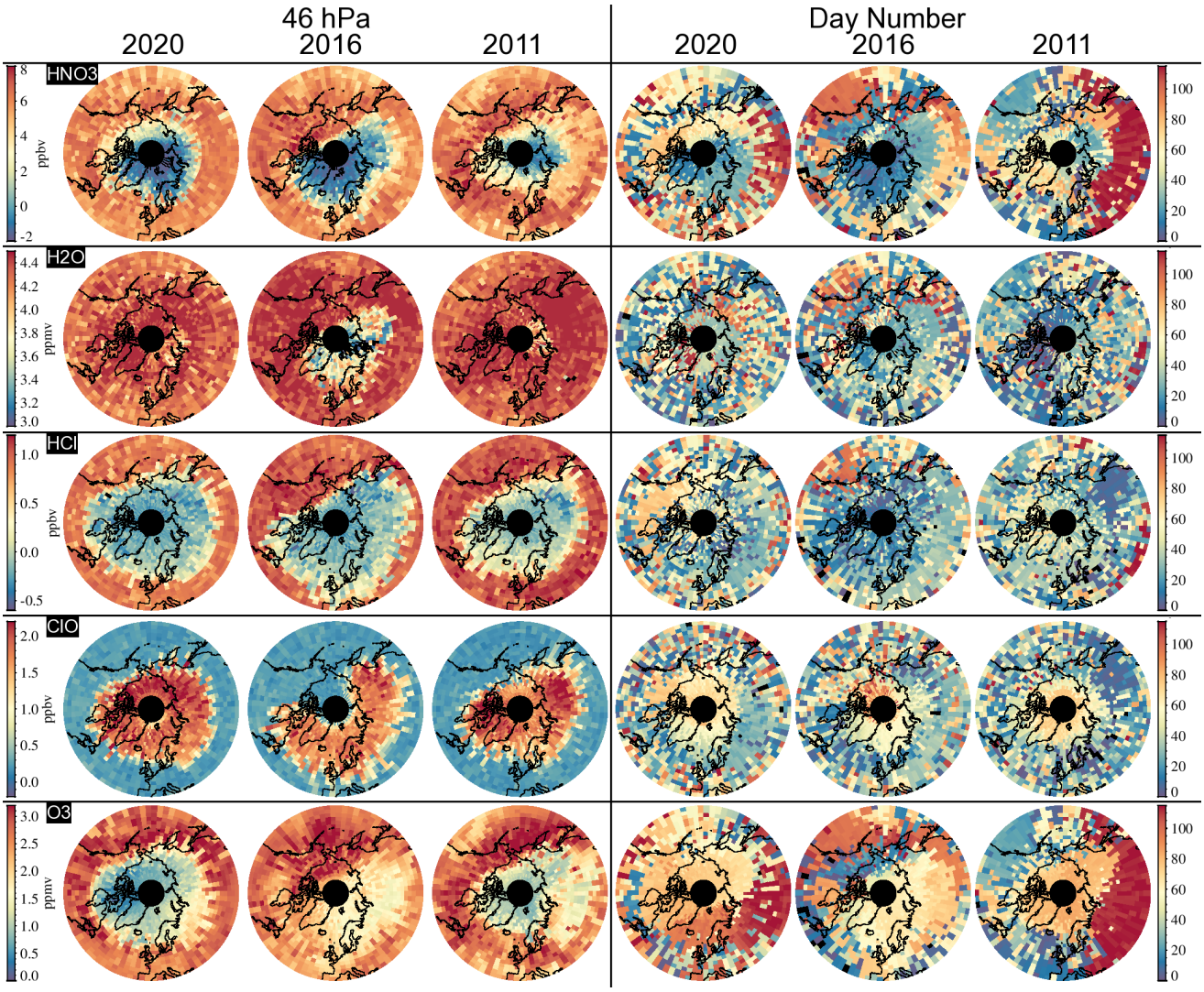

Figure S2. As in Fig. S1, but at 46 hPa.

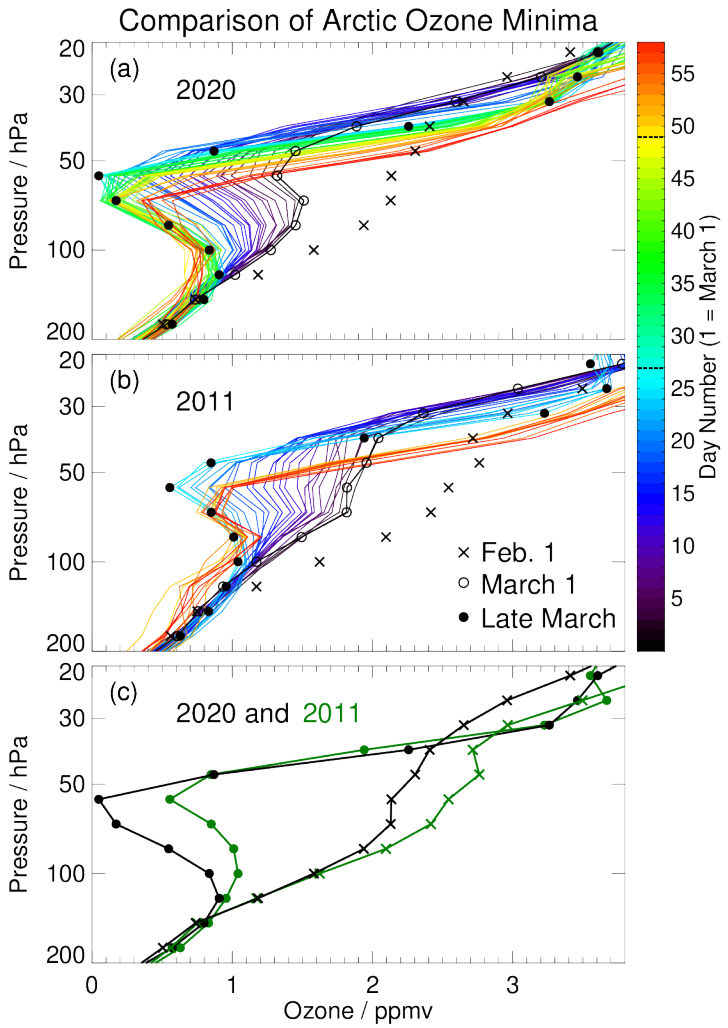

Figure S3. Minimum ozone mixing ratios for Arctic profiles in 2020 and 2011. Minima are obtained by considering the lowest 5% of the average mixing ratios between 82 and 46 hPa, covering the MLS ozone retrieval pressure levels with largest ozone decreases during February and March. (a) Minimum profiles for 2020, with 1 February (x-es), 1 March (open circles), and the lowest minimum in February/March (filled circles), in this case 27 March (day number 27 on the color bar). For clarity, we are not showing the minimum profiles before 1 March. (b) Same as (a) except for 2011; in this case, the minimum profile observed was on March 25; the color bar indicates (dashed horizontal lines) the range of days for which no MLS data were available (MLS was turned off from 27 March though 18 April). (c) Comparison of minima on 1 February (x-es) and in late March (filled circles) between 2020 (black) and 2011 (green).

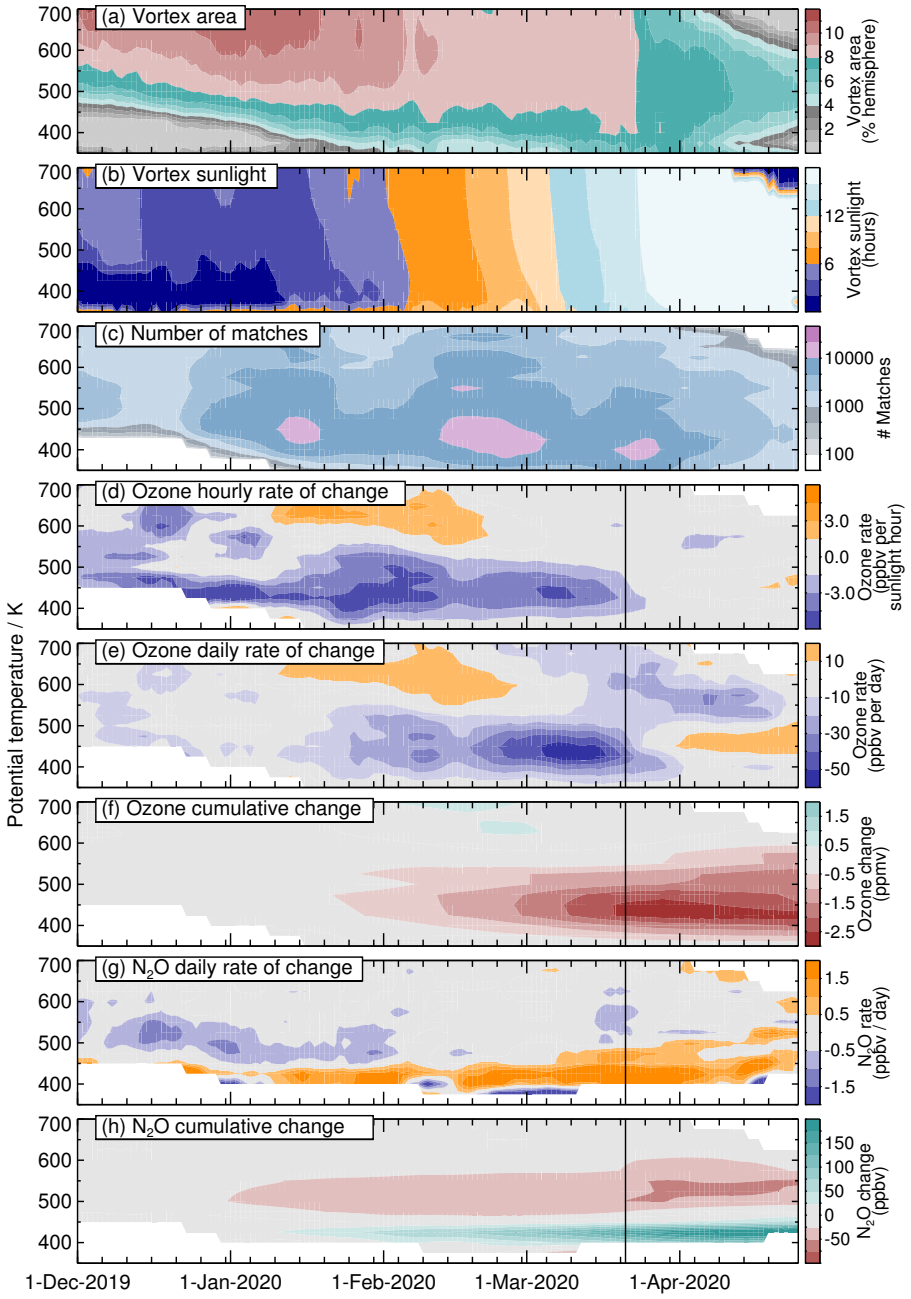

Figure S4. Temporal evolution of various height-resolved quantities during the 2019/2020 Arctic winter: (a) Polar vortex area (vortex edge defined per (Lawrence et al., 2018), with an offset of $+0.2\times10^{-4}$ s^{-1} as discussed above), expressed as a fraction of a hemisphere. (b) Average daily sunlight exposure time of air within the vortex. (c) Number of MLS matches in the vortex within a 15-day moving window in 25 K-thick potential temperature layers. (d) Estimated ozone loss rate per sunlight hour. (e) estimated daily ozone loss rate. (f) Cumulative ozone change. (g) N_2O daily rate of change. (h) N_2O cumulative change.

May 27, 2020, 7:43pm

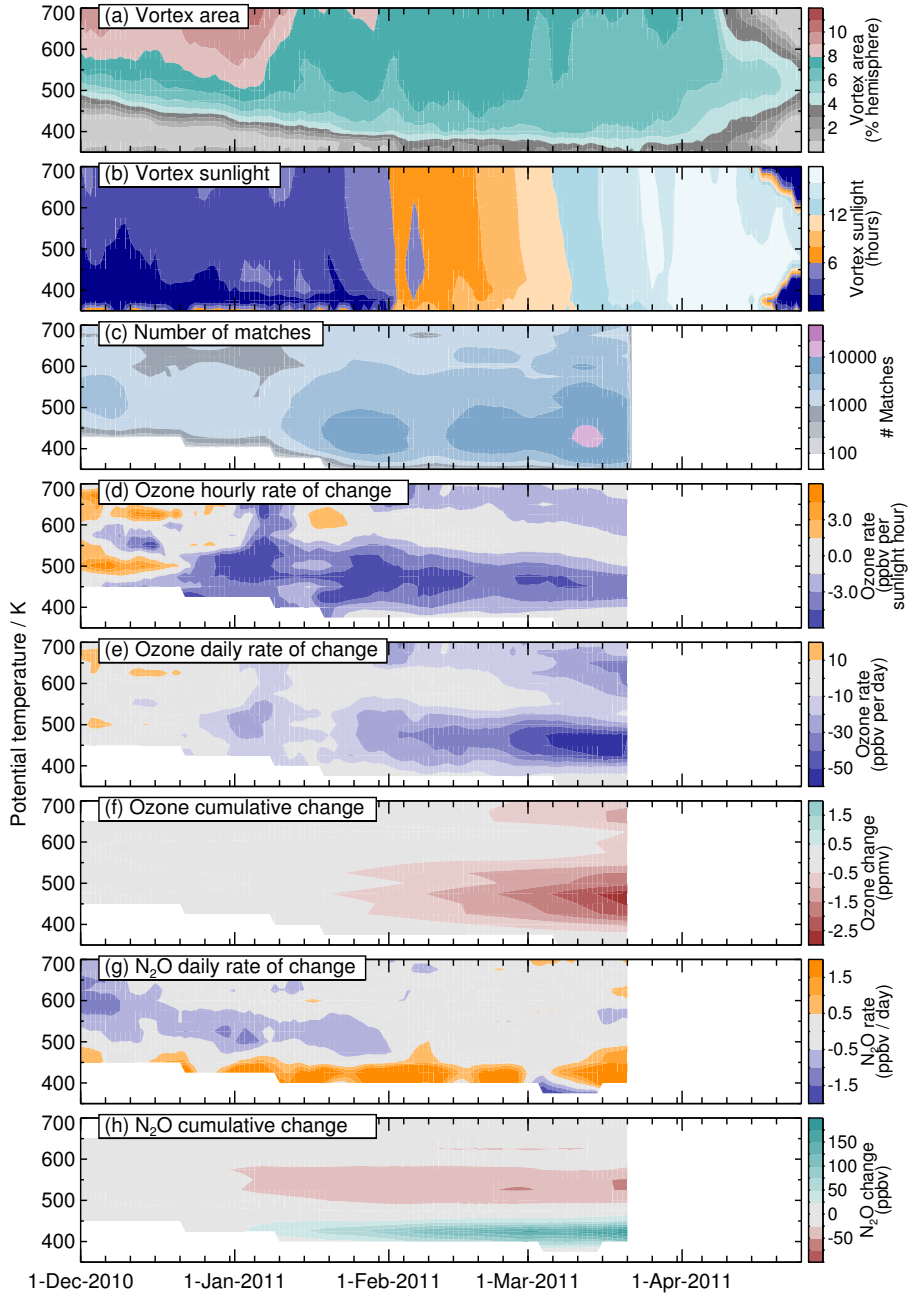

Figure S5. As Figure S4 but for the 2010/2011 Arctic winter/spring.